

Rotating Drops of Axion Dark Matter

Sacha Davidson ^{1,*} and Thomas Schwetz ^{2,†}

¹*Univ. Lyon, Université Lyon 1, CNRS/IN2P3, IPN-Lyon, F-69622, Villeurbanne, France*

²*Institut für Kernphysik, Karlsruher Institut für Technologie (KIT), D-76021 Karlsruhe, Germany*

Abstract

We consider how QCD axions produced by the misalignment mechanism could form galactic dark matter halos. We recall that stationary, gravitationally stable axion field configurations have the size of an asteroid with masses of order $10^{-13}M_{\odot}$ (because gradient pressure is insufficient to support a larger object). We call such field configurations “drops”. We explore whether rotating drops could be larger, and find that their mass could increase by a factor ~ 10 . Remarkably this mass is comparable to the mass of miniclusters generated from misalignment axions in the scenario where the axion is born after inflation. We speculate that misalignment axions today are in the form of drops, contributing to dark matter like a distribution of asteroids (and not as a coherent oscillating background field). We consider some observational signatures of the drops, which seem consistent with a galactic halo made of axion dark matter.

1 Introduction

The QCD axion [1, 2] is a motivated, minimal and very curious dark matter candidate. It originally appeared [3] in Peccei and Quinn’s solution to the strong CP problem [4], as the pseudo-goldstone boson of a global, anomalous $U_{PQ}(1)$ symmetry. In “invisible” axion models [5, 6] which agree with observations, heavy new scalars and/or fermions are introduced, and the $U_{PQ}(1)$ is spontaneously broken at a high scale $f_{PQ} \sim 10^9 \rightarrow 10^{11}$ GeV, so that the only new particle at accessible energies is the light, feebly-coupled axion. And despite that the axion and neutrino have comparable masses, the axion is a cold dark matter candidate, due to its non-thermal production in cosmology.

There are two production mechanisms for axion cold dark matter, in the case where the Peccei-Quinn phase transition occurs after inflation. Both occur around the QCD phase transition, when the axion mass turns on. The “misalignment mechanism” [7, 8], produces an oscillating classical axion field, and the decay of the string network produces a distribution of cold axion modes. The classical field, produced by the misalignment mechanism, will be called “the axion field” in the following. This may be what some authors refer to as a Bose Einstein Condensate, however, the literature is confusing because other authors discuss whether the misalignment axions could “gravitationally thermalise”, as a prerequisite to forming a Bose Einstein Condensate.

In this paper, we focus on the axion field, despite that most axion dark matter may be produced by strings [9, 10]. As pointed out by Sikivie [11], dark matter composed of an axion field is different from WIMPs. The T^{ij} elements (pressures) of the stress-energy tensor are different, and the axion field is single-valued, whereas WIMPs are described by a phase space distribution. The difference is intuitive and clear during late-time structure formation: particles (described by phase space) fall into a gravitational well, rise up the other side, fall back, and so on. Indeed the whole population of particles does this simultaneously, interacting only via gravity in the usual CDM approximation. This can be modelled via N-body simulations. The axion field, being single-valued, is like a fluid, so its velocity must remain single-valued as it falls in, possibly leading to shocks and turbulence.

The original aim of this project was to address the question “How to make the halo of Andromeda (or any other galaxy) with the QCD axion field?”. This is both a dynamical question, about the evolution of axion dark matter from the QCD phase transition until today, and a “stationary” question, about the axion field configuration in the galaxy over the past several billion years. Sections 2 and 3 address the “stationary” part of the question. We give approximate solutions of the equations of motion of the axion and Newtonian gravity, and call these self-gravitating solutions “drops”. Such solutions have been studied for a wide range of parameters, in the literature for “Bose stars” [12, 13] and galactic halos [14, 15]. They are discussed very completely by Rindler-Daller and Shapiro (RDS) [14] and Chavanis, Chavanis and Delfini [15], where can be found extensive references. As pointed out by Barranco and

*E-mail address: s.davidson@ipnl.in2p3.fr

†E-mail address: schwetz@kit.edu

Bernal [16], and noticed by several authors [14, 15], the mass and size of QCD axion drops is $M \sim 10^{-13} M_\odot$ and $R \sim 100$ km, which is small compared to Andromeda ($M \sim 10^{12} M_\odot$, $R \sim 100$ kpc)¹. Chavanis [15] showed that the negative self-interaction of QCD axions gives an upper bound of this order on the size of a non-rotating drop. We allow our drops to rotate, and find by analytic estimates (section 2) as well as numerical solutions of the relevant equations (section 3) that rotating drops can be about one order of magnitude more massive.

Section 4 reviews the history of the Universe in the scenario where the Peccei-Quinn phase transition occurs after inflation. Hogan and Rees [17] noticed that in this scenario, there are $\mathcal{O}(1)$ fluctuations in the energy density of the axion field on the scale of the horizon at the QCD phase transition. The mass of these fluctuations, referred to as “miniclusters” can be comparable or larger than the axion drop mass. So we use the virial theorem to hypothesize that, when miniclusters gravitationally collapse, the larger ones fragment into axion drops. (The collapse of miniclusters should be addressed numerically, which we hope to do shortly.) If this is the case, then the axion field dark matter in the Universe today would be in the form of axion drops, which would behave as WIMPs [16]. In particular, this implies that in the neighbourhood of the sun, any coherently oscillating background axion field is small, and is not determined by the dark matter density, with possibly severe implications for axion dark matter searches [18].

Section 5 reviews the constraints on dark matter in the form of axion drops, which are within the mass range of “macro dark matter”, studied in [19]. We summarize in section 6. In the appendix we provide a derivation of the non-relativistic field equations coupled to Newtonian gravity, starting from the general relativistic action of a real scalar field.

2 The axion “drop”: a stable gravitationally bound configuration

The aim of this section is to identify stable configurations of the QCD axion field, in the presence of self-interactions and Newtonian gravity. We refer to these configurations as “drops”². This question has been widely studied [14, 15, 16, 20, 21]; our new contribution is to allow the drops to rotate. We review analytic estimates for the mass and radius of the drops, as a function of the various microscopic and/or external parameters ($m, f_{\text{PQ}}, m_{\text{P1}}, \dots$), which imply that the drops resemble asteroids. The purpose of the analytic estimates is to understand how the mass and radius of the drops scale; so the estimates only need to be of the right order of magnitude.

The drops may rotate, but we neglect time-variation of the radial density profile. This means that our drop is not allowed a “breathing mode”, which could be compatible with long-term stability; we suppose that this would not significantly change the parameters we are interested in.

The stress-energy tensor for the real QCD axion field a is $T_\nu^\mu = a^{;\mu} a_{;\nu} - [\frac{1}{2} a^{;\alpha} a_{;\alpha} - V(a)] \delta_\nu^\mu$, where the potential after the QCD phase transition, is³

$$V(a) \approx f_{\text{PQ}}^2 m^2 [1 - \cos(a/f_{\text{PQ}})] \simeq \frac{1}{2} m^2 a^2 - \frac{1}{4!} \frac{m^2}{f_{\text{PQ}}^2} a^4 + \frac{1}{6!} \frac{m^2}{f_{\text{PQ}}^4} a^6 + \dots \quad (1)$$

and the axion mass is

$$m \simeq \frac{m_\pi f_\pi}{f_{\text{PQ}}} \frac{\sqrt{m_u m_d}}{m_u + m_d} \simeq 10^{-4} \text{ eV} \frac{6 \times 10^{10} \text{ GeV}}{f_{\text{PQ}}}. \quad (2)$$

In this paper, we take $m \simeq 10^{-4}$ eV, because in the scenario where the Peccei-Quinn phase transition is after inflation, the numerical simulations of Kawasaki, Saikawa and Sekiguchi [10] (hereafter KSS) suggest that this gives the correct dark matter abundance. f_{PQ} is the breaking scale of the Peccei-Quinn symmetry, here taken to be fixed in terms of the axion mass by eqn (2). The potential (1) is therefore a one-parameter potential determined by m .

In the non-relativistic limit, the real axion field can be written in terms of a complex field ϕ [23]

$$a = \frac{1}{\sqrt{2m}} (\phi e^{-imt} + \phi^* e^{imt}) = \frac{1}{\sqrt{2m}} (\eta e^{-i(S+mt)} + \eta e^{i(S+mt)}), \quad (3)$$

with η and S real. It is intuitive that a real field becomes complex in the non-relativistic limit, because particle number is conserved. The potential for the non-relativistic field is

$$V(\phi) = \frac{m}{2} \phi^* \phi - \frac{g}{2} |\phi|^4 + \dots, \quad \frac{g}{2} = \frac{1}{16 f_{\text{PQ}}^2} \quad (4)$$

¹Recall that $M_\odot = 1.1 \times 10^{57} \text{ GeV} = 2.0 \times 10^{30} \text{ kg}$, $\text{kpc} = 3.086 \times 10^{21} \text{ cm}$.

²We thank a seminar participant at Zurich University for this name.

³We adopt in this paper the dilute-instanton approximation for the potential, which suffices for our purposes. A recent discussion of some modifications can be found in [22].

(obtained by dropping the terms that oscillate as $e^{\pm iNmt}$, on the assumption that they average to zero), and the field ϕ satisfies a Schrödinger-type equation

$$i\dot{\phi} = -\frac{\nabla^2}{2m}\phi - |g|(\phi^\dagger\phi)\phi + mV_N\phi \quad , \quad \text{GP equation} \quad (5)$$

(obtained by neglecting ∂_t^2 and $(\partial_t)^2$ terms in the Klein-Gordon equation for a , see appendix for a derivation). Note that in “natural units” ϕ and g have mass dimension 3/2 and -2 , respectively, while the Newtonian potential V_N is dimensionless⁴. Equation (5) is referred to as the Gross-Pitaevski (GP) equation, and is widely used, from describing Bose Einstein condensation of cold atoms to galaxy halos made of $m \sim 10^{-20}$ eV bosons. A useful review about this equation is [26].

The dynamics of the axion field coupled to gravity can be obtained from $T^{\mu\nu}_{;\nu} = 0$, or from the Klein Gordon equation. The axion $T^{\mu\nu}$ is parametrised by the axion energy density ρ and fluid three-velocity \vec{v} , which are more intuitive variables for Large-Scale-Structure (LSS) than the field. The transformation between these two parametrisations is discussed in the works of Chavanis[15] and Rindler-Daller and Shapiro (RDS) [14]. The stress-energy tensor for the non-relativistic axion field, in cartesian coordinates for flat space-time (Newtonian gravity can be added later by hand), is

$$\begin{aligned} T_{00} &= \rho = m\eta^2 + \dots \\ T_{0i} &= \eta^2\partial_i S + \dots = -\rho v^i + \dots \\ T_{ij} &= \frac{1}{2m} \left(2\partial_i\eta\partial_j\eta + 2\eta^2\partial_i S\partial_j S + \delta_{ij}[-\nabla\eta\nabla\eta + 2m\eta^2\dot{S} - \eta^2\nabla S\nabla S + m|g|\eta^4] \right) \end{aligned} \quad (6)$$

$$= \frac{\partial_i\rho\partial_j\rho}{4m^2\rho} + \rho v_i v_j - \delta_{ij} \left[\frac{\nabla^2\rho}{4m^2} - \frac{|g|}{2m^2}\rho^2 \right] \quad (7)$$

where the equations of motion were used to simplify the brackets between the first and second lines for T_{ij} , and we defined $v^j = -\partial_j S/m$.

Two equations are obtained from $T^{\mu\nu}_{;\nu} = 0$:

$$\partial_t\rho = -\nabla \cdot \rho\vec{v} \quad \text{continuity} \quad (8)$$

$$\rho\partial_t\vec{v} + \rho\vec{v} \cdot \nabla\vec{v} = \rho\nabla \left(\frac{\nabla^2\sqrt{\rho}}{2m^2\sqrt{\rho}} + |g|\frac{\rho}{m^2} - V_N \right) \quad \text{Euler} \quad (9)$$

which can also be obtained from the real and imaginary parts of the complex GP equation (5) by using $\phi = \sqrt{\frac{\rho}{m}}e^{-iS}$ and $v^j = -\partial_j S/m$, and taking the divergence of the real equation. The gravitational potential V_N is obtained from the Poisson Equation

$$\nabla_x^2 V_N(x - x') = 4\pi G_N \rho(x') \quad , \quad (10)$$

which outside a spherical mass distribution, has the familiar solution $V_N(r) = -G_N M(r)/r$ with $M(r)$ being the mass inside the radius r .

From the Euler equation, one can already see that a stationary solution (neglecting rotation, so setting the left side of Euler to zero) should balance the outwards gradient pressure represented by the first term, against the inwards gravitational and self-interaction pressures. The self-interaction pressure is inwards because the density decreases with r , so $\partial_r\rho < 0$. An estimate for the mass M and radius R of an axion drop can be obtained by replacing $\nabla \rightarrow 1/R$, $\rho \rightarrow M/R^3$ on the right-hand-side of the Euler equation, and solving the resulting quadratic equation for R :

$$\left(\frac{1}{2m^2 R^2} - |g|\frac{M}{m^2 R^3} - G_N \frac{M}{R} \right) \simeq 0 \quad \Rightarrow \quad R \sim \frac{m_{\text{Pl}}^2}{4m^2 M} \quad , \quad M \lesssim \frac{m_{\text{Pl}} f_{\text{PQ}}}{m} \quad . \quad (11)$$

This exhibits an upper bound on the drop mass, as found by Chavanis, as well as the usual “virial” relation between the radius and mass of an object supported against gravity by pressure. Below we will use the virial theorem to obtain a more reliable equation, but this already indicates the parametric dependence of the mass and radius of the drop. Notice that the maximum drop mass $\propto 1/m^2$, so lighter axions can form larger drops. Solving for R at the maximum mass $M \sim 10^{-14} M_\odot$, gives $R \sim 100$ km.

More sophisticated estimates are obtained, for instance, by Chavanis or RDS, by guessing a functional form for $\rho(\vec{r})$, and minimising the energy functional that gives the GP equation. RDS consider bosons of variable mass and

⁴Recall that eqn (5) is a classical field equation, so it contains no \hbar , despite its formal similarity to the Schrödinger equation. Setting $c = 1$ (time in units of distance d), the dimensions are $[\phi] = \sqrt{E}/d$, $[g] = d/E$ and $[m] = 1/d$, where E is energy or mass. In particular, the parameter m of the classical field is an inverse length, and \hbar is required to relate it to the mass of quanta of the field [24, 25].

positive self-interaction (which provide an outward pressure, helpful in obtaining cores for galactic halos), and find rotating field configurations which could be galactic halos for bosons of mass $m \sim 10^{-20}$ eV. Chavanis considers variable masses and self-interactions of either sign, and looks for non-rotating solutions. For a QCD axion (negative self-interaction), and a non-rotating drop, Chavanis found a maximum mass of $10m_{\text{Pl}}f_{\text{PQ}}/m$, by minimising an energy functional with an exponential ansatz for the radial profile of the density.

Estimates similar to eqn (11) can be obtained using the virial theorem. It says, for a stationary, spherically symmetric space-time [27]

$$\frac{3}{2} \int Pr^2 dr d\Omega = \int G_N \frac{\rho M(r)}{r} r^2 dr d\Omega \quad (12)$$

where $3P = \sum_i T^{ii}$. This can be written in the form used by Chavanis and RDS

$$E_{\text{grav}} + 2E_{\text{cin}} + 3E_{\text{si}} = 0, \quad (13)$$

where

$$E_{\text{grav}} = \int dV \frac{\rho}{2} V_N, \quad E_{\text{si}} = g \int dV \frac{\rho^2}{2m^2}, \quad E_{\text{cin}} = \frac{1}{2} \int dV \left[\frac{(\nabla \rho)^2}{4\rho m^2} + \rho |\vec{v}|^2 \right]. \quad (14)$$

We assume in this paper, following RDS, that a rotating axion drop should also satisfy the virial condition eqn (13). We consider rotating drops of axion field, and estimate whether the rotation could allow them to be significantly more massive than the estimate of eqn (11). To obtain an ansatz for the rotating drop, notice the resemblance between the (non-linear) GP equation and the (linear) Schrodinger equation for the Hydrogen atom, the latter having well-known solutions in terms of spherical harmonics. It is convenient to start from the axion field, rather than ρ and \vec{v} , because the phase of the field should be continuous, and this condition is less simple to impose on ρ and \vec{v} . Following Tkachev [28], we suppose the rotating axion drop has the functional form in radial coordinates

$$\phi(r, \theta, \varphi) = \sqrt{\frac{\rho_c}{m}} F(r) Y_l^l(\theta, \varphi), \quad Y_l^l = c_l \sin^l \theta e^{il\varphi}, \quad c_l = \frac{(-1)^l}{2^l l!} \sqrt{\frac{(2l+1)!}{4\pi}} \quad (15)$$

where c_l is taken such that $\int |Y_l^l|^2 d\Omega = 1$, which ensures that the total mass of the drop is independent of l and remains $\sim \rho_c r_c^3$. For simplicity, the radial function $F(r)$ is taken to give a density of top-hat form:

$$\rho(r, \theta) = |c_l|^2 \rho_c \theta (r_c - r) \sin^{2l} \theta, \quad (16)$$

in which case the total mass of the drop is $M = \rho_c r_c^3 / 3$.

Various comments can be made.

1. The radial density profiles $F(r)$ contain two parameters: a central density ρ_c (integrated over angles), and r_c which is some measure of the size of the drop. In addition to the top-hat, we tried an ‘‘isothermal-sphere-squared’’ profile, $F(r) = r_c^2 / (r^2 + r_c^2)$, because it approaches being a solution of the static Euler equation and has a finite volume integral. These results are not given, because they only differ from the top-hat profile in irrelevant numerical factors (despite that the integration is more involved).
2. A solution of the Schrödinger equation is usually expanded on the set of $\{Y_n^l\}$. We select one Y_l^l for simplicity; the equations of motion are non-linear, so this allows to avoid products $Y_n^l Y_{n'}^{*l}$. In addition, the parametrisation $\phi = \sqrt{\frac{\rho}{m}} e^{-iS} \propto Y_l^l$, $\vec{v} = -\nabla S / m$, relates l to the fluid velocity $v_r = 0, v_\theta = 0, v_\varphi = l / (mr \sin \theta)$. Note that in the case of a single Y_n^l the choice Y_l^l with $n = l$ corresponds to choosing the z -axis of the coordinate system along the angular momentum vector.
3. Asteroids in our solar system can have masses and radii comparable to the non-rotating axion drops, and tend to have rotation periods ~ 6 hours. However, their formation history differs from that of axion drops, so it is unclear whether this is a relevant analogy. The equatorial rotation frequency of a drop described by eqn (15), evaluated at the radius r_c , would be $\omega \simeq l / (r_c^2 m) \simeq 6l / \text{day}$, which suggests that low l values are realistic.
4. With the ansatz of eqn (15), the parameter l describes two distinct physical aspects of the drop: its rotation, and also its flattening into a disk. However, we allow this degeneracy, because we only consider l values of order a few, due to the previous point.

To obtain the gravitational energy which enters the virial condition (13), the potential $V_N(r, \theta)$ is required. Expanding the density on spherical harmonics, $\rho(r, \theta) = \rho(r) \sum_{k \leq 2l} \eta_k Y_0^k(\theta)$ with $\eta_k = \int d\Omega \sin^{2l} \theta Y_0^k$, the potential is [29]

$$V_N(r, \theta) = -4\pi G_N \sum_k \frac{\eta_k Y_0^k(\theta)}{2k+1} \left(\frac{1}{r^{k+1}} \int_0^r da a^{k+2} \rho(a) + r^k \int_r^\infty \frac{da}{a^{k-1}} \rho(a) \right) \equiv -4\pi G_N \sum_k V_k(r) Y_0^k(\theta) \quad (17)$$

which illustrates the interest of the top-hat density profile. This gives

$$\begin{aligned} E_{grav} &= -2\pi G_N \sum_k \int_0^\infty r^2 \eta_k \rho(r) V_k(r) dr \\ &= -\frac{4\pi G_N}{15} \rho_c^2 r_c^5 |c_l|^4 \left\{ |\eta_0|^2 + \frac{3|\eta_2|^2}{5} + \sum_{4 \leq k \leq 2l} \frac{3|\eta_k|^2}{(k+3)(2k+1)} \right\} \\ &\gtrsim -\frac{4\pi G_N}{15} \rho_c^2 r_c^5 \frac{|c_l|^4}{|c_{2l}|^2} \rightarrow -\frac{3G_N M^2}{5r_c} \sqrt{1+l} \end{aligned} \quad (18)$$

where, in the last approximation, the curly brackets were taken $\leq \sum_k |\eta_k|^2 = 1/|c_{2l}|^2$, and after the arrow approximates⁵ $\frac{|c_l|^4}{|c_{2l}|^2} \simeq \sqrt{l+1}/4\pi$. The kinetic and self-interaction energies are

$$3E_{si} = -\frac{M^2}{r_c^3} \frac{9}{16f_{\text{PQ}}^2 m^2} \frac{|c_l|^4}{|c_{2l}|^2} \rightarrow -\frac{M^2}{r_c^3} \frac{9}{64\pi f_{\text{PQ}}^2 m^2} \sqrt{1+l} \quad (19)$$

$$2E_{cin} = \frac{3M}{8m^2 r_c^2} [1 + 4l(l+1)], \quad (20)$$

using $(\partial\rho/\partial r)^2 \simeq \rho_c^2 |c_l|^4 \sin^{4l} \theta \delta(r - r_c)/r$.

We see that the gravitational and self-interaction energies grow as $\sqrt{l+1}$. This is because the drop flattens into a disk for large l (as a result of our ansatz (16)), so the density is larger to stay at constant mass. The kinetic energy grows quadratically with l , both because the drop has angular momentum, and because of the gradient in θ . Solving the Virial equation for r_c gives

$$Mr_c \simeq \frac{5m_{\text{P1}}^2}{8m^2} \frac{1 + 4l(l+1)}{\sqrt{l+1}} \left[1 \pm \sqrt{1 - \frac{3(l+1)m^2 M^2}{5\pi [1 + 4l(l+1)]^2 f_{\text{PQ}}^2 m_{\text{P1}}^2}} \right] \Rightarrow M \lesssim \sqrt{\frac{5\pi}{3}} \frac{m_{\text{P1}} f_{\text{PQ}}}{m} \frac{1 + 4l(l+1)}{\sqrt{l+1}} \quad (21)$$

which, for $l = 0$, reproduces the parametric dependence of the estimates obtained from the Euler equation in eqn (11). However, the constants are unreliable, because Chavanis obtained a maximum mass of $\sim 10^{-13} M_\odot$ with an exponential ansatz for the radial density profile of a spherically symmetric solution. So we suppose the upper bound is

$$M \lesssim \frac{1 + 4l(l+1)}{\sqrt{l+1}} \times 10^{-13} M_\odot. \quad (22)$$

For $l \sim \text{few}$, which corresponds to the rotation rates of asteroids, the maximum mass of the drop can grow by an order of magnitude or so. This behaviour is confirmed by the numerical calculations presented in the next section.

The upper bound on the size of the drop arises because the self-interaction energy of the QCD axion is negative (equivalently, it exerts an inwards force, like gravity): if the mass M inside a volume $\sim R^3$ is to high, the gradients cannot compensate the self-interaction energy. However, the QCD axion has a cosine potential, see eqn (1), and not the unbounded-below $-|g||\phi|^4$ potential used to compute E_{si} . So one can wonder whether the maximum mass is an artifact of expanding the potential. It seems no: a more correct version of the potential, in the non-relativistic approximation where the mass term does not appear, would be $m^2 f_{\text{PQ}}^2 [1 - \cos(a/f_{\text{PQ}})] - m^2 a^2/2$. This is also always negative, and well-approximated by $-m^2 a^4/(4! f_{\text{PQ}}^4)$ at the maximal drop mass (which corresponds to $a/f_{\text{PQ}} \sim f_{\text{PQ}}/m_{\text{P1}} \ll 1$). So drops beyond the maximal mass would collapse⁶ or fragment. Ref. [16] shows by numerical calculation that the 6th order term in the potential has a small impact on the density profile.

⁵ For $l = \{0, 1, 2, 3, \dots\}$, $\frac{|c_l|^4}{|c_{2l}|^2} = \{1, \frac{5}{6}, \frac{5}{7}, 1.63, \dots\} \times \frac{1}{4\pi}$. For large l , the Stirling approximation for large- n factorials, $n! \simeq \sqrt{2\pi n} \left(\frac{n}{e}\right)^n$, gives $\frac{|c_l|^4}{|c_{2l}|^2} = \sqrt{\frac{2l}{\pi}} \frac{1}{4\pi}$.

⁶ One could wonder if there are smaller, heavier drops, whose radius could be estimated by balancing the inward self-interaction pressure from $m^2 f_{\text{PQ}}^2 [1 - \cos(a/f_{\text{PQ}})] - m^2 a^2/2$, against the outwards gradients. However, the radius where this self-interaction energy balances the gradient energy can be estimated to be $\sim 1/m$.

3 Numerical solution of the GPP system

In this section we are solving the coupled Gross-Pitaevski [eqn (5)] and Poisson [eqn (10)] equations numerically. We proceed in analogy to the standard treatment of the hydrogen atom. We make an ansatz for the field in terms of a radial wave function $R(r)$ and spherical harmonics:

$$\phi = R(r)Y_m^l(\vartheta, \varphi)e^{-iEt}, \quad M = m \int_0^\infty dr r^2 R^2(r), \quad (23)$$

(so $R(r) = \sqrt{\frac{\rho_c}{m}}F(r)$ in eqn (15)). In general ϕ may consist of a superposition of various Y_m^l . As before, we assume here for simplicity that the field consists just of a single Y_m^l with given lm . As usual, thanks to the factor e^{-iEt} we obtain a time-independent Schrödinger equation:

$$ER = \left\{ -\frac{1}{2m} \left[\Delta_r - \frac{l(l+1)}{r^2} \right] + mV_N - |g|R^2|Y_m^l|^2 \right\} R, \quad (24)$$

where Δ_r is the radial part of the Laplace operator in polar coordinates. Note that this equation still depends on ϑ and φ via the potential V_N and the self-interaction term. Therefore, we take the angular average of eqn (24). We define the angular averaged gravitational potential and use the normalization of the spherical harmonics:

$$\bar{V}_N(r) \equiv \frac{1}{4\pi} \int d\Omega V_N(r, \vartheta, \varphi), \quad \int d\Omega |Y_m^l|^2 = 1. \quad (25)$$

Then we obtain for the angular averaged GP and Poisson equations:

$$\Delta_r R = \left[2m(m\bar{V}_N - E) + \frac{l(l+1)}{r^2} - |g|\frac{m}{2\pi}R^2 \right] R \quad (26)$$

$$\Delta_r \bar{V}_N = G_N m R^2, \quad (27)$$

which now are just two coupled second order differential equations for the two functions $R(r)$ and $\bar{V}_N(r)$.

We can make this system dimensionless and absorb the coupling constants g and G_N , the axion mass m , and the constant E by appropriate rescaling:

$$\Delta_{\tilde{r}} \tilde{R} = \left[\tilde{V}_N + \frac{l(l+1)}{\tilde{r}^2} - \tilde{R}^2 \right] \tilde{R} \quad (28)$$

$$\Delta_{\tilde{r}} \tilde{V}_N = \tilde{R}^2, \quad (29)$$

with

$$r = \frac{1}{m} \sqrt{\frac{|g|}{4\pi G_N}} \tilde{r}, \quad R = 2\pi \frac{\sqrt{2G_N m}}{|g|} \tilde{R}, \quad \bar{V}_N - \frac{E}{m} = \frac{2\pi G_N}{|g|} \tilde{V}_N, \quad (30)$$

where the tilde quantities are dimensionless. Using $m_{\text{Pl}} = 1/\sqrt{G_N} \approx 1.2 \times 10^{19}$ GeV and the QCD expression for g given in eqn (4) we can write those relations as

$$r = \frac{1}{4\sqrt{2\pi}} \frac{m_{\text{Pl}}}{m f_{\text{PQ}}} \tilde{r} \approx 4 \times 10^4 \text{ m } \tilde{r}, \quad R = 16\sqrt{2\pi} \frac{m^{1/2} f_{\text{PQ}}^2}{m_{\text{Pl}}} \tilde{R}, \quad \bar{V}_N - \frac{E}{m} = 16\pi \frac{f_{\text{PQ}}^2}{m_{\text{Pl}}^2} \tilde{V}_N. \quad (31)$$

The total mass of the axion drop is given as

$$M = 2\sqrt{2\pi} \frac{m_{\text{Pl}} f_{\text{PQ}}}{m} \tilde{M} \sim 10^{-13} M_\odot \left(\frac{f_{\text{PQ}}}{10^{11} \text{ GeV}} \right)^2 \tilde{M} \quad \text{with} \quad \tilde{M} = \int_0^\infty d\tilde{r} \tilde{r}^2 \tilde{R}^2. \quad (32)$$

Assuming that tilde quantities are of order one, eqs (31) and (32) set the scales for the typical dimensions of the axion drop, in agreement with the estimates of the previous section. This confirms that one obtains the same physics by studying either the equations of motion for the field, or Einsteins equations for the stress-energy tensor. We can also estimate the typical density of the drop as

$$\rho(r) = mR^2(r) \approx 3 \text{ g cm}^{-3} \left(\frac{f_{\text{PQ}}}{10^{11} \text{ GeV}} \right)^2 \tilde{R}^2(r), \quad (33)$$

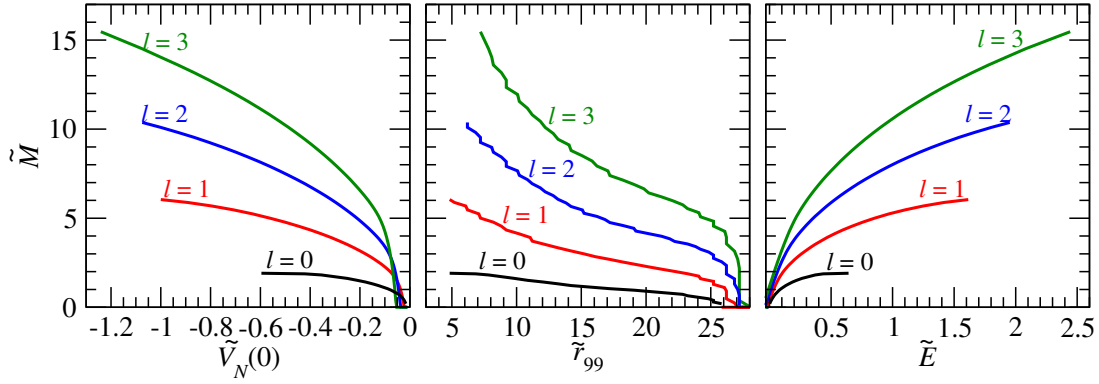


Figure 1: A set of solutions of the GPP system for $l = 0, 1, 2, 3$. The 3 panels show the total mass as a function of the initial values for \tilde{V}_N (left), as a function of the radius containing 99% of the mass (middle), and \tilde{E} (right). The initial value $\tilde{R}(0)$ has been fixed at 10^{-2} for $l = 1$ and at 10^{-4} for $l = 2, 3$, while for $l = 0$ it has a finite value. The relation of the dimensionless quantities shown in the plots to physical quantities is given in Eqs (31), (32), (36).

which is comparable to the average density of the Earth for this choice of f_{PQ} .

Now the task is to numerically solve the GPP system (28), (29). These are 2 second order differential equations for the functions $\tilde{R}(\tilde{r})$ and $\tilde{V}_N(\tilde{r})$. We need to specify 4 initial conditions: $\tilde{R}(0), \tilde{R}'(0), \tilde{V}_N(0), \tilde{V}_N'(0)$, with prime denoting derivative with respect to \tilde{r} .

For a given $R(r)$ we can integrate the Poisson equation (29) and obtain a solution for the potential:

$$\tilde{V}_N(\tilde{r}) = -\frac{1}{\tilde{r}} \int_0^{\tilde{r}} dx x^2 \tilde{R}^2(x) - \int_{\tilde{r}}^{\infty} dx x \tilde{R}^2(x) + \tilde{E}. \quad (34)$$

Here \tilde{E} is an integration constant. Another integration constant has been chosen such that we obtain the following limiting expressions:

$$\tilde{V}_N(0) = -\int_0^{\infty} dx x \tilde{R}^2(x) + \tilde{E}, \quad \tilde{V}_N(\tilde{r} \rightarrow \infty) = -\frac{\tilde{M}}{\tilde{r}} + \tilde{E} \rightarrow \tilde{E}. \quad (35)$$

This choice of integration constants implies that $\tilde{V}_N(\tilde{r})$ is finite at $\tilde{r} = 0$ and $\tilde{V}_N'(0) = 0$. At distances far away from the mass distribution we obtain the Newtonian result for the potential in physical units, $V_N(r) = -G_N M/r$, when we identify

$$\tilde{E} = -\frac{|g|}{2\pi G_N} \frac{E}{m} = -\frac{1}{16\pi} \frac{m_{\text{Pl}}^2}{f_{\text{PQ}}^2} \frac{E}{m}. \quad (36)$$

Considering the GP equation at large radii and requiring that $R(r)$ decreases exponentially we find that \tilde{E} should be positive, i.e., $E < 0$. In the familiar Schrödinger equation for the hydrogen atom, E would be the binding energy of the electron. We find this analogy useful, despite that, in our classical field theory, the energy is a volume integral and E has units of frequency. As shown below, for the solutions we have $\tilde{E} \lesssim 1$. Hence it follows

$$-\frac{E}{m} \lesssim 16\pi \frac{f_{\text{PQ}}^2}{m_{\text{Pl}}^2} \approx 3.5 \times 10^{-15} \left(\frac{f_{\text{PQ}}}{10^{11} \text{ GeV}} \right)^2 \quad (37)$$

and $|E| \ll m$, which justifies the nonrelativistic treatment.

Our procedure is now as follows: We set $\tilde{V}_N'(0) = 0$ and pick some values for $\tilde{R}(0)$ and $\tilde{V}_N(0)$. Then we search for $\tilde{R}'(0)$ by a shooting method, such that for the solution \tilde{R}, \tilde{R}' and \tilde{V}_N go to zero at large \tilde{r} . If a solution is found we can then calculate the corresponding total mass \tilde{M} , the radius containing 99% of the mass, \tilde{r}_{99} , and \tilde{E} . In Fig. 1 we show the behaviour of the total mass of the drop, \tilde{M} , for the cases $l = 0, 1, 2, 3$. Beyond the point where the curves stop we could not find any solution with physical boundary conditions, indicating the existence of a maximal possible mass. When we try to extend the curves beyond the maximal mass, the solutions diverge at large radii. In Fig. 2 (left panel) we show the radial profiles for the maximal mass for each l value. For those solutions we required zero nodes of $\tilde{R}(r)$.

For $l > 0$ physically interesting solutions have vanishing wave function at the centre, since the angular momentum term in the GP equation diverges as $r \rightarrow 0$ for finite $R(0)$. For the numerics, we fix \tilde{R} at 0.01 for $l = 1$ and at 10^{-4}

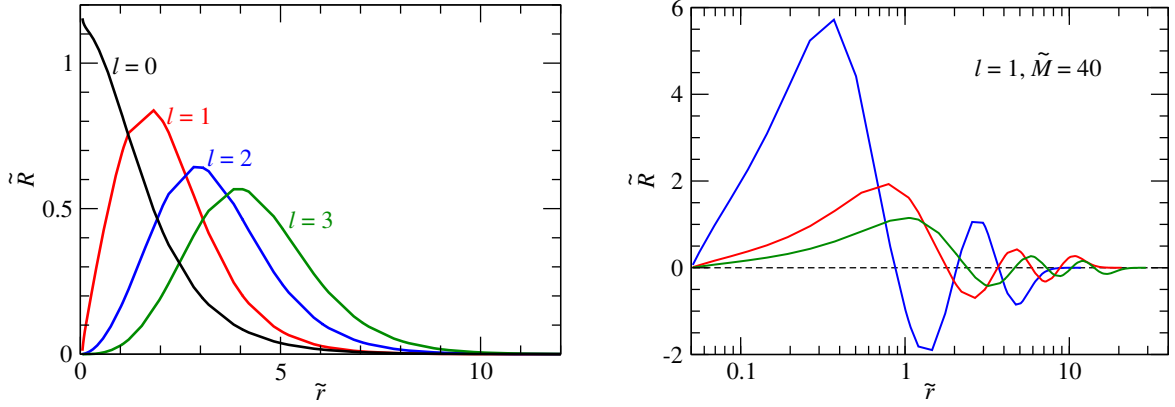


Figure 2: Left: The radial wave function $\tilde{R}(\tilde{r})$ for the solutions for $l = 0, 1, 2, 3$ corresponding in each case to the maximum mass shown in figure 1. Right: Radial wave function for solutions for $l = 1$ with 3, 4, and 5 nodes, where all three examples correspond to a total mass $\tilde{M} \approx 40$.

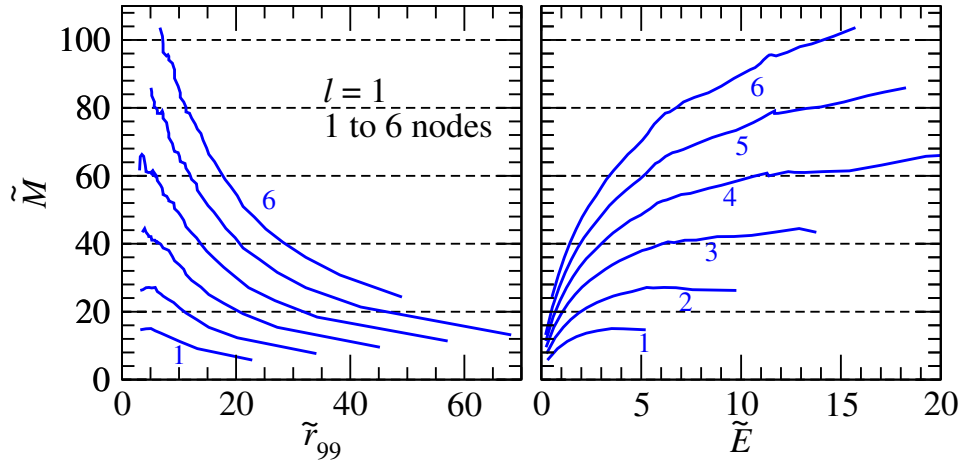


Figure 3: Solutions for $l = 1$ with 1 to 6 nodes of the radial wave function (curves from bottom up have increasing number of nodes). We show the total mass \tilde{M} as a function of \tilde{r}_{99} (left) and \tilde{E} (right).

for $l = 2, 3$ at radius $\tilde{r} = 0.05$ and then we scan different values of $\tilde{V}_N(0)$. For each value we search for the derivative $\tilde{R}'(0)$ in order to obtain a physically interesting solution, converging at large radii. For $l = 0$, $\tilde{R}(0)$ is non-zero and we have to scan also over this parameter, in addition to $\tilde{V}_N(0)$ and $\tilde{R}'(0)$.

Our results for the $l = 0$ case are in qualitative agreement with figs. 4 and 5 from [21]. However, so far we could not find solutions with smaller \tilde{r}_{99} as the one corresponding to the maximal mass (cf. fig. 4 of [21]) or equivalently larger $\tilde{R}(0)$ (cf. fig. 1 of [30]). Note that to search for $l = 0$ solutions we have restricted the derivative $\tilde{R}'(0)$ to be small (the condition we impose is $|\tilde{R}'(0)| < \tilde{R}(0)$). If we allow for large derivatives at small radii solutions are found for different combinations of $\tilde{R}(0)$ and $\tilde{V}_N(0)$. Those allow also for slightly larger total masses, although qualitatively the behaviour is similar to the shown solutions.

We find that the solutions for $l > 0$ are more massive than in the $l = 0$ case by about a factor 3 for $l = 1$, a factor 5 for $l = 2$, and a factor 8 for $l = 3$, but the size increases only slightly, from $\tilde{r}_{99} \approx 5$ to 7. Restricting to solutions with zero nodes we did not find any solution for $l \geq 4$.

In Fig. 3 we show solutions with 1 to 6 nodes for the case with $l = 1$. We observe that significantly larger masses can be obtained for multi-node solutions. Fig. 2 (right panel) shows three examples for the wave function with $l = 1$ and 3, 4, and 5 nodes. For all three examples the total mass is approximately $\tilde{M} \approx 40$. We have also searched for multi-node solutions with higher values of l . As in the zero-node case, we have not found physical solutions for $l \geq 4$.

The results of our numerical study of the GPP system can be summarized as follows.

1. We recover the well known result from the literature that for the “ground state” with zero nodes and $l = 0$ there is a maximal possible mass, let’s call this maximal mass of the ground state \tilde{M}_0^{\max} .

2. For a given mass, solutions with lower angular momentum l and less nodes have larger \tilde{E} and hence are favoured. However, for masses $\tilde{M} > \tilde{M}_0^{\text{max}}$, there seems to be a minimal l and (for given l) a minimal number of nodes, for which solutions exist. Hence, if we look for a solution for a fixed mass with $\tilde{M} > \tilde{M}_0^{\text{max}}$, the solution with the maximum \tilde{E} is obtained at $l > 0$ and/or with a non-zero number of nodes.
3. We have not found solutions with $l \geq 4$; this may be an artifact of our single Y_m^l approximation, or may indicate an upper bound on the angular momentum of the drop. It deserves further study.

In this paper we have not considered the question of stability of solutions against small perturbations. Ref. [31] has found that for the non-interacting and non-rotating case, only the ground-state with zero-nodes is stable, whereas solutions with nodes are unstable with respect to oscillations, see also [13]. We leave the stability analysis of multi- l and multi-node solutions for the QCD axion case for future investigations. This question needs to be addressed as well within the dynamical framework of the formation of the axion drops.

4 From the QCD phase transition till today

4.1 Estimating the minicluster mass

We suppose that the Peccei-Quinn phase transition occurs after inflation, leaving a massless axion field which is random from one horizon-volume to the next, a network of cosmic strings, and no domain walls. Shortly before the QCD phase transition, the axion mass is expected to turn on, generating the potential (1). This leads to two axion contributions to dark matter:

1. It causes the network of cosmic strings to decay. This process is simulated numerically [9, 32, 33]; the recent results of KSS [10] give two comparable contributions to axion dark matter. From the Peccei Quinn phase transition until the axion mass turns on, the string network radiates axions with $p \sim H$. Then domain walls form between the strings, separating regions of $\pm a$, and subsequently this wall-string network decays away to axions with $p \sim m(T) \sim H$.
2. The axion field, random in each horizon-volume, is likely to be misaligned with respect to the minimum of the potential, so will roll down and oscillate. The initial magnitude of the field, averaged over many horizons, is $\pi f_{\text{PQ}}/\sqrt{3}$. The oscillations redshift like cold dark matter [7, 8, 34].

Combining these contributions to axion dark matter, KSS [10] obtained an appropriate relic density for $m \sim 10^{-4}$ eV. Only $\sim 25\%$ of this CDM is due to the misalignment field, the remainder is in the incoherent distribution of axion modes produced by strings.

In this paper, we are interested in the misalignment axion field, which can have two types of density fluctuations. It inherits the large-scale adiabatic density fluctuations present in radiation, which will later grow into the observed Large Scale Structure. More interesting for us, are the short-distance, isocurvature “miniclusters”, originally discussed by Hogan and Rees [17], and extensively studied by Kolb and Tkachev [35]. These arise because the axion field is random, from one horizon to the next, as the axion mass turns on before the QCD PT. This gives $\mathcal{O}(1)$ density fluctuations on the QCD horizon scale, which are frozen in the expanding radiation until matter-radiation equality, then decouple from the Hubble expansion and collapse.

We want to estimate the mass of a minicluster. This will depend on the coherence length and energy density of the axion field, evaluated as the axion mass turns on. The temperature dependence of the axion mass is equivalent to the topological susceptibility $\chi(T)$ of the QCD plasma, which has been widely studied. Here we consider three possible behaviours for $m^2(T)$ prior to the QCD phase transition. In the interacting instanton liquid of [36], the temperature-dependent axion mass can be written

$$m(T) = c \frac{\Lambda_{\text{QCD}}^2}{f_{\text{PQ}}} \left(\frac{\Lambda_{\text{QCD}}}{T} \right)^{n/2}, \quad (38)$$

with $\Lambda_{\text{QCD}} = 400$ MeV, and where $c = 4 \times 10^{-4}$, $n = 6.68$. (The zero-temperature mass is obtained for $n = 0$, $c = 4 \times 10^{-2}$, and $m(T)$ should stop growing when it reaches the zero-temperature mass.) The instanton liquid gives a less-steep turn-on than dilute instanton gas estimates [37, 34], and is the parametrisation used by KSS [10] to estimate that $m \sim 10^{-4}$ eV gives the correct relic density of axion CDM today. A recent lattice-based estimate [22] suggests that the axion mass could turn on more slowly, with $c \simeq 3 \times 10^{-3}$, $n \simeq 2$, whereas the lattice-based analysis of Kitano and Yamada [38] explored the possibility that the axion mass turns on exponentially at the critical temperature $T_c \simeq 150$ MeV.

Once the axion mass reaches its zero temperature value m , the minicluster mass can be estimated as

$$M_{mini} \sim V_{osc} m(T=0) n_{osc} E, \quad (39)$$

where T_{osc} is the temperature when $m(T_{osc}) = 3H(T_{osc})$, V_{osc} and n_{osc} are the volume of the horizon and the comoving axion number density at that moment, and E is an enhancement factor which takes into account that the axion field is inhomogeneous so starts to oscillate at different times in different horizons. We take $V_{osc} \sim 1/[8H^3(T_{osc})]$ and $n_{osc} \sim m(T_{osc})f_{\text{PQ}}^2 \langle \theta_i^2 \rangle \approx m(T_{osc})f_{\text{PQ}}^2 \pi^2/3$. It is reasonable to take the minicluster volume to be V_{osc} , because recall that the field was initially random on much smaller scales, and is smoothed to the horizon-scale by the dynamics of a massless scalar field. The enhancement factor E arises because, in horizons where $a \sim \pi f_{\text{PQ}}$, the axion potential does not have a $m^2 a^2$ form, and the beginning of oscillations (with the associated $1/R^3$ red-shifting of the energy density) is delayed. Several studies [37, 39, 34] have estimated $E \sim 2 \rightarrow 8$ by numerically solving the equations of motion⁷. However it is unclear in these analyses, whether the field gradients are included in the equations of motion. The gradients are explicitly included in the analysis [35], who find that the axion field could remain trapped at $a \sim \pi f_{\text{PQ}}$ while the temperature dropped by an order of magnitude. However, the $a \sim \pi f_{\text{PQ}}$ configurations of this analysis may correspond to the domain walls that form between strings, after the axions get a mass, and whose decay is studied by KSS [10]. We take $E = 8$. (This may be large, but other authors take the horizon volume to be $V = 1/H^3$. We have $EV = 1/H^3$.) This leads to

$$M_{mini} \sim \frac{\pi^2 m f_{\text{PQ}}^2}{H^2(T_{osc})}. \quad (40)$$

With the parameters corresponding to the interacting instanton liquid of [36], and $f_{\text{PQ}} \simeq 6 \times 10^{10}$ GeV as found by KSS, we find the axion starts to oscillate around $T \sim 1 \rightarrow 2$ GeV, giving

$$M_{mini} \sim 3 \times 10^{-13} M_{\odot}. \quad (41)$$

This is similar to the value found in [45], but smaller than the original estimate of Hogan and Rees [17], whose miniclusters formed at $T = 100$ MeV in a CDM-dominated Universe. In the case of the more gradual turn-on of the axion mass advocated in [22], the axion starts to oscillate sooner ($T_{osc} \sim \text{few GeV}$), so the miniclusters could be an order of magnitude smaller. If the axion mass turns on exponentially at the QCD phase transition, as discussed in [38], then it is possible that the axion would contribute to much CDM. Requiring that the observed dark matter density is due to axions in this scenario, the axion could start to oscillate at $T \sim \Lambda_{\text{QCD}}$, giving miniclusters an order of magnitude or so larger.

Interestingly, M_{mini} of eqn (41) is not so different from the maximum mass of a stable drop estimated in eqn (22). This appears to be an accident: the maximum mass of a drop is determined by balancing the kinetic pressure against the gravitational and self-interaction forces — whereas the mass of a minicluster is determined by the volume of the horizon when the axion starts to oscillate. To see why these are similar, recall that the axion starts to oscillate when $3H(T_{osc}) \sim m(T_{osc})$. Replacing $25mf_{\text{PQ}} \sim \Lambda_{\text{QCD}}^2$ in eqn (38), gives

$$M_{mini} \sim \frac{\pi^3 m f_{\text{PQ}}^2}{H(T_{osc})} \frac{1}{m(T_{osc})} \sim \pi^3 m f_{\text{PQ}}^2 \frac{m_{\text{Pl}}}{15T^2} \frac{4T^2}{m^2 f_{\text{PQ}}} \left(\frac{T}{25mf_{\text{PQ}}} \right)^{\frac{n-4}{4}} \sim \frac{f_{\text{PQ}} m_{\text{Pl}}}{m} \frac{8T^{1.34}}{\Lambda_{\text{QCD}}^{1.34}}$$

where the last estimate used $n/2 = 3.34$, for which the last fraction is ~ 50 . The estimates of the minicluster and drop masses, given in eqns (41) and (22), are both very uncertain. In both cases, formation is a dynamical process which should generate a spectrum of masses. So we take these estimates to have an uncertainty of at least an order of magnitude, and conclude that the average minicluster mass could be of order the maximum drop mass, or a hundred times larger.

4.2 Speculations on how to make Andromeda

We can now speculate on how axion dark matter could make the Andromeda galaxy, in the case where the Peccei-Quinn phase transition occurs after inflation.

After the QCD phase transition, there are two contributions to axion dark matter: the misalignment field, and the incoherent distribution of modes produced by strings. It is convenient to refer to this phase space distribution of modes as “particles”, to distinguish it from the misalignment field (distributions of classical waves evolve in a way very

⁷Notice that E is the enhancement in the density of overdense regions, whereas often the enhancement in the average density is given.

similar to distributions of particles [40]). Once the axion mass has settled to its zero-temperature value, the particles are non-relativistic, with velocity $\sim H(\Lambda_{\text{QCD}})/m \sim 10^{-5}c$ (for $m = 10^{-4}$ eV). Despite their small mass, these particles should be sufficiently “cold” to virialise and form a galactic halo of particles with $v \sim 0.001c$.

There are two types of density perturbations that can arise in the field and in the particles. On large scales, they both inherited from the surrounding radiation, the scale-free, adiabatic density fluctuations produced during inflation. Then, due to the dynamics at the QCD phase transition, the field has $\mathcal{O}(1)$ density fluctuations on the QCD horizon scale (~ 0.03 pc today), which give a white noise spectrum ($\delta M/M \sim \sqrt{M_{\text{mini}}/M}$) of density fluctuations on small scales. These are the miniclusters. The particles might also have a similar small-scale spectrum. These density fluctuations are frozen into the radiation plasma until they dominate the radiation density (see *e.g.* [41]). At matter-radiation equality, the large-scale fluctuation which will eventually become Andromeda, which has an initial amplitude $\delta\rho/\rho \lesssim 10^{-4}$, can start to grow. Meanwhile, the short-distance $\mathcal{O}(1)$ inhomogeneities, such as miniclusters, decouple from the Hubble flow and collapse.

We now focus on the small-scale inhomogeneities in the field. A realistic and accurate calculation of minicluster formation would give a spectrum: the number density of miniclusters as a function of their mass. Those with mass less than the maximum allowed for drops should initially collapse to axion drops. Hogan and Rees [17] speculate that miniclusters undergo hierarchical clustering, however it is unclear to us how this would occur: do small drops amalgamate to form larger drops, or do the drops cluster like dark matter particles?

In the case that a minicluster exceeds the maximum drop mass, the virial theorem suggests that the miniclusters fragment into stable drops. The point is that the virial condition implies that the (negative) gravitational energy gained in collapse should be compensated by kinetic energy, so one can anticipate that the minicluster fragments into smaller field configurations, in the presence of steep field gradients. This would of course require numerical verification. The alternative is that the minicluster collapses to a black hole. However, it is often argued that $\mathcal{O}(1)$ density fluctuations should be of horizon-scale in order to collapse to black holes [42], which is not the case for miniclusters.

In this paper, we do not consider small-scale inhomogeneities in the density of axions produced by strings. The string network is very inhomogeneous, but decays to relativistic axion particles [10], which become non-relativistic as the temperature-dependent axion mass increases towards its zero-temperature value. The degree to which the particle density becomes smooth by free-streaming, prior to the axions becoming non-relativistic, is unclear (to us). Kolb and Tkachev explored this question [45], using a dilute instanton gas approximation for $m(T)$, and argue that the axions from strings also have $\mathcal{O}(1)$ density fluctuations on the QCD horizon scale. This corresponds to the original analysis of Hogan and Rees [17], where the miniclusters were assumed to be composed of axion particles. Hogan and Rees estimate that the cores of miniclusters could survive the hierarchical merging of miniclusters and the galaxy formation process, but that a significant fraction of axion particles would be thrown off, and would today contribute a smooth halo density of axion particles, as could for instance be detected by axion dark matter search experiments such as ADMX [18].

On the other hand, if a significant fraction of axion dark matter is in the form of drops, this would reduce the signal in direct detection. Denoting the mass fraction of axion drops to the smooth halo component by f_{drop} , we expect a number density of drops with mass $10^{-13} M_{\odot}$ of order $f_{\text{drop}} \times 10^{-44} \text{ cm}^{-3}$, which implies about $f_{\text{drop}} \times 10^{-5}$ drops in a volume of $(1 \text{ AU})^3$ and a drop flux on Earth of $f_{\text{drop}} \times 10^{-34} \text{ cm}^{-2} \text{ s}^{-1}$. (We have assumed a local dark matter density of 0.4 GeV cm^{-3} and a drop velocity in the galactic halo of $10^{-3} c$.) Hence, ADMX would see only the smooth component of the halo, which will be reduced by a factor $(1 - f_{\text{drop}})$.

5 Observational bounds

The observational signatures of “macroscopic” dark matter objects, with masses from grams to several solar masses were recently compiled in [19]. The case of primordial black holes is reviewed in [43]; while black holes created with $M \lesssim 10^{-18} M_{\odot}$ would evaporate in the lifetime of the Universe, there is a window [44] $10^{-13} M_{\odot} \lesssim M_{\text{PBH}} \lesssim 10^{-9} M_{\odot}$ where they could constitute the dark matter (the lower bound is from femtolensing, the upper bound from microlensing). This window is interesting, because in the case that large miniclusters collapsed to black holes, they would be in this allowed range. Kolb and Tkachev [45] discussed the sensitivity of femto- and pico-lensing experiments axion miniclusters. Zurek et al [46] consider astrophysical effects of miniclusters in the wide range of $10^{-12} \rightarrow 10^4 M_{\odot}$. Here we suppose that axion field dark matter is in the form of drops, with $M \lesssim 10^{-13} \rightarrow 10^{-12} M_{\odot}$ and review the femtolensing bound. Other possible constraints are listed.

5.1 Femtolensing

Micro-lensing is the familiar idea of watching nearby stars (*e.g.* in the LMC), in the hope of observing an increase in their light due to a compact halo object crossing the line of sight. Femtolensing [47] uses Gamma Ray Bursters (GRBs) as sources, which are at cosmological distances, and most of which only last for a few seconds. The lensing objects are therefore distributed in intervening galaxies and intergalactic space. And rather than looking for an amplification in light signal, one looks for the interference between light that took two different paths round the lensing object: the time delay between the two paths is the same for photons of different energies, so one looks for oscillations in the energy spectrum of GRBs.

Femtolensing is an idea of Gould [47], that lensing by dark objects with $10^{-16}M_{\odot} \lesssim M \lesssim 10^{-13}M_{\odot}$ could give interference patterns in the energy spectrum of GRBs. A bound based on BATSE data [48], could exclude $\Omega \sim 0.2$ for the mass range $10^{-16} \rightarrow 10^{-13}M_{\odot}$, and these authors also estimated picolensing bounds, and found a 1σ sensitivity to $\Omega \sim 1$ of compact objects in the mass range $10^{-12.5}M_{\odot} \rightarrow 10^{-9}M_{\odot}$. In a careful and dedicated analysis of FERMI data, Barnacka et al [49] focussed on GRBs at measured redshift, and were able to exclude $\Omega > 0.03$ in compact objects of mass between $5 \times 10^{-17} \rightarrow 5 \times 10^{-15}M_{\odot}$, which is somewhat below the maximum drop mass estimated in eqn (22).

The exclusion of [49] assumes that the GRB can be treated as point source. Otherwise, various photons emitted by the GRB could have different time delays in their paths around the lens (because they come from different locations on the source), and the oscillations in the intensity-summed-over-photons could be washed out [47]. The GRB can be treated as point source provided that its “size”, projected onto the lens plane, is smaller than the Einstein radius $r_E = 2\sqrt{G_N M(D_{OL}D_{LS}/D_{OS})}$, where the distances D are between Observer, Source and Lens. It is unclear, from the estimates in [49], that this condition is satisfied (such doubts were expressed in [50]). Furthermore, the GRB size estimates in [51] are one or two orders of magnitude larger than those in [49]. It would be helpful if the status of these constraints was confirmed by expert authors.

5.2 Other constraints?

Axion drops as dark matter could have many other observable consequences, due to their interactions with the CMB, magnetic fields, or other astrophysical objects, due to their passage in our local area, and so on. Some possibilities are listed here. Questions which arise, for some of these constraints, are whether the drop accretes baryons (see *e.g.* [46]), and how it interacts with photons (discussed in [52]).

1. Carr and Sakkelariadou [53] considered dynamical constraints on compact objects, which could disrupt the structures we see. They expect that compact objects in the mass range $10^{-18} \rightarrow 10^{-11}M_{\odot}$ could resemble comets. From the non-observation of interstellar comets in the past 300 years, they impose that no compact objects (CO) passed through a disk of radius one earth-sun distance (astronomical unit= AU) in 300 years, which implies, following [54]:

$$M > \frac{\Omega_{\text{CO}}}{\Omega_{\text{DM}}} 10^{-13}M_{\odot}. \quad (42)$$

So for drop masses $\gtrsim \text{few} \times 10^{-14}M_{\odot}$, this observation does not pose a constraint. Whether there is a bound on smaller drops would require study, to determine whether they shine like baryonic comets.

2. There are constraints on DM-photon interactions from CMB observations, for instance as given in [55] — it would be interesting to understand if these apply to axion drops? In [19], it is argued that macroscopic compact objects have a geometric cross-section with photons, and can be subject to the same “collisional damping” (Silk damping) constraints as particle dark matter. Whether this is the case for drops might depend on whether they accumulate baryons.
3. Do the drops evaporate due to self-interactions?

The rate at which four axions from the condensate (field) could evaporate into two particles with energy $\sim 2m$ is estimated⁸ in [8] as $\sim m^3 a^6 / f_{\text{PQ}}^4$. For $a/f_{\text{PQ}} \sim f_{\text{PQ}}/m_{\text{Pl}}$, as obtained in the axion drop, this evaporation timescale is much longer than the age of the Universe.

The decay of axion drops due to emission of real axions because of the the self-interaction term via a $3a \rightarrow a$ process has been studied in [56]. This process becomes kinematically allowed when the whole axion drop balances momentum. It has been found that if configurations close to the maximal possible total mass of the drop are

⁸This can be simply obtained as the $2 \rightarrow 2$ scattering rate with an effective four-point coupling $m^2 a^2 / f_{\text{PQ}}^6$.

considered, the decay becomes relevant for axion masses around $\lesssim 10^{-8}$ eV, but should be unimportant for $m \sim 10^{-4}$ eV, as implied by $f_{\text{PQ}} \sim 10^{11}$ GeV.

Axion particles in the galactic halo (originally produced by string decay), could scatter axions out of the drops. The rate for this process was estimated in [57] to be $\sim n_a m^2 / f_{\text{PQ}}^4 \times f_{\text{BE}}$, where f_{BE} is a Bose enhancement factor that accounts for the high occupation number of the axion particles, which can locally be estimated as $f_{\text{BE}} \sim 0.3 \text{ GeV} / (m^4 v^3 \text{ cm}^3) \sim 10^{20}$ (for $v \sim 0.001c$ the local virial velocity). The fraction of axions scattered out of drops in the age of the Universe τ_U is therefore $\sim (m f_{\text{BE}} / m_{\text{Pl}}) \ll 1$.

4. One can ask what happens if a drop meets an ordinary star, a white dwarf, a neutron star, or a black hole. Collisions of axion drops with white dwarfs and neutron stars [58] have been proposed as a source for GRBs, as well as to explain other anomalies. However the energy released in the collision of a drop with a neutron star is controversial [30] (as is also the case for the interactions of primordial black holes with neutron stars [50, 59, 60]).
5. The ‘‘explosion’’ of axion drops was recently proposed as a possible source for Fast Radio Bursts [61].

6 Summary

Dark matter composed of the QCD axion can be produced either by the misalignment mechanism, giving rise to an axion field, or by the decay of strings, which produces a distribution of axion modes/particles. We consider stable axion field configurations, held together by gravity and self-interactions, and confirm that they have typical dimensions of 100 km and a mass scale $M \sim 10^{-13} M_\odot \sim 10^{-7} M_\oplus \sim 10^{17}$ kg. The maximum mass of the drop arises from balancing the inward gravity and self-interaction pressures against kinetic gradient pressure.

We allowed the axion drops to rotate, and found that the maximum mass can increase by about an order of magnitude. This result is estimated analytically in section 2 using the virial theorem, and obtained in section 3 from numerical solutions of the classical field equations. In both cases we have assumed that the axion field in the drop is proportional to a single spherical harmonic $Y_m^l(\vartheta, \varphi)$. In realistic situations one may expect that the field is a general linear combination of several Y_m^l . Nevertheless, our simplified ansatz indicates that modestly rotating drops ($l \lesssim \text{few}$) may be somewhat heavier than non-rotating configurations.

In this work, we looked for stable solutions, but did not study the dynamical process of drop formation (which would depend on the earlier cosmological evolution). Nonetheless, in section 4, we speculate on how axion drops could arise if the Peccei-Quinn phase transition occurs after inflation. In this scenario, the misalignment axions are only a component of the dark matter, and have $\mathcal{O}(1)$ inhomogeneities on the horizon scale of the QCD phase transition which are referred to as miniclusters. The estimated mass of miniclusters is slightly larger than the maximum mass of stable axion drops, so we envisage that the miniclusters could fragment into drops. On the other hand, if the Peccei-Quinn phase transition occurs before inflation, then the misalignment axions compose all the axion dark matter, but there are no miniclusters, and it is an open question whether large-scale density fluctuations would fragment on small scales into drops.

In section 5, we reviewed observational constraints on dark matter in the form of asteroid sized objects, and it appears that dark matter halos made of axion drops could be consistent with observations. Interesting constraints close to the relevant mass range are obtained by femtolensing. Several other potential constraints depend whether axion drops accrete baryons, which we did not study.

It is interesting to speculate on the implications of axion drops for direct detection experiments, such as ADMX [18]. Recall that in the cosmological scenario where the Peccei-Quinn phase transition occurs after inflation, current numerical simulations [10] suggest that $\sim 75\%$ of axion dark matter is composed of particles produced by strings. As reviewed at the end of section 4.2, these axion particles could provide a smooth halo component, as searched for by ADMX. However, the dark matter fraction stored in drops would be hidden from axion direct detection experiments.

Acknowledgements

SD thanks Georg Raffelt for useful, pleasant, and essential discussions.

A Non-relativistic approximation

In general a scalar field coupled to gravity is described by the following action

$$S = \int d^4x \sqrt{-g} \left[\frac{\mathcal{R}}{16\pi G_N} + \mathcal{L} \right], \quad (43)$$

where $g \equiv \det(g_{\mu\nu})$ is the determinant of the metric and \mathcal{R} is the Ricci scalar. We consider here the Langrange density of the relativistic real axion field a of the form

$$\mathcal{L} = -\frac{1}{2}g^{\mu\nu}(\partial_\mu a)(\partial_\nu a) - V(a), \quad V(a) = \frac{1}{2}m^2 a^2 - \frac{1}{4!}\lambda a^4, \quad (44)$$

with the dimensionless quartic coupling $\lambda = m^2/f_{\text{PQ}}^2$. When the action is extremized with respect to the metric $g_{\mu\nu}$ and the field a one obtains the coupled Klein-Gordon and Einstein equations. Here we are going to derive the non-relativistic limit, where all velocities are small compared to c and energies small compared to m . We follow closely Ref. [23].

For the metric we take the Newtonian ansatz with

$$g_{00} = -(1 + 2V_N), \quad g_{i0} = 0, \quad g_{ij} = (1 - 2V_N)\delta_{ij}, \quad (45)$$

with the Newtonian potential $V_N(\vec{x}) \ll 1$ and we neglect the explicit time dependence of V_N . Hence, we have $\sqrt{-g} \approx 1 - 2V_N$. To leading order in V_N the Ricci scalar is given by $\mathcal{R} = -2(\partial_i V_N)^2$ (see for instance [62] eqn 5.17 with metric definition 4.9), and we obtain for the action

$$S = \int d^4x \left[-\frac{(\partial_i V_N)^2}{8\pi G_N} + \frac{1 - 4V_N}{2}\dot{a}^2 - \frac{1}{2}(\partial_i a)^2 - (1 - 2V_N)V(a) \right], \quad (46)$$

with dot denoting time derivative. In order to take the non-relativistic limit for the axion we write the real relativistic field a in terms of a complex non-relativistic field ϕ as in eqn (3). The non-relativistic approximation assumes that ϕ varies only slowly on time scales $1/m$:

$$\dot{\phi} \ll m\phi, \quad \ddot{\phi} \ll m\dot{\phi}, \quad (47)$$

and all factors containing exponentials $e^{\pm imt}$ average to zero when integrated over t in the action. Note that with the ansatz for ϕ from eqn (23) the above approximation just means $E \ll m$, which has been confirmed to hold for our solutions, see eqn (37). Under these assumptions we find

$$\dot{a}^2 \rightarrow i(\dot{\phi}\phi^* - \dot{\phi}^*\phi) + m\phi\phi^*, \quad (\partial_i a)^2 \rightarrow \frac{1}{m}(\partial_i \phi)(\partial_i \phi^*), \quad a^2 \rightarrow \frac{1}{m}\phi\phi^*, \quad a^4 \rightarrow \frac{3}{2m^2}(\phi\phi^*)^2. \quad (48)$$

In the expression for \dot{a}^2 we have neglected a term $\phi^*\dot{\phi}/m$ but kept the ones with only one derivative. Then we obtain the action in terms of the fields V_N, ϕ, ϕ^* :

$$S = \int d^4x \left[-\frac{(\partial_i V_N)^2}{8\pi G_N} + \frac{i}{2}(\dot{\phi}\phi^* - \dot{\phi}^*\phi) - mV_N\phi\phi^* - \frac{1}{2m}(\partial_i \phi)(\partial_i \phi^*) + \frac{(1 - 2V_N)\lambda}{16m^2}(\phi\phi^*)^2 \right]. \quad (49)$$

We have neglected terms of order $V_N\dot{\phi}\phi^*$ compared to $mV_N\phi\phi^*$ according to eqn (47). Note that the large terms of order $m\phi\phi^*$ cancel, as a consequence of factoring out the fast oscillations with frequency m , which basically reduces the Klein-Gordon equation to the Schrödinger equation. Applying Euler-Lagrange equations for ϕ^* to the action (49) we find the GP equation, eqn (5), with $g = \lambda/(8m^2) = 1/(8f_{\text{PQ}}^2)$, see eqn (4), and we neglect the gravitational potential $V_N \ll 1$ in the term proportional to λ .

The Euler-Lagrange equations for V_N lead to the following equation:

$$\Delta V_N = 4\pi G_N \left(m + \frac{\lambda}{8m^2}\phi\phi^* \right) \phi\phi^*. \quad (50)$$

Apart from the second term in the bracket this is the Poisson equation eqn (10). Let us use the results of section 3 to estimate the relative size of the two terms in the bracket:

$$\frac{\lambda}{8m^3}\phi\phi^* = \frac{1}{8} \frac{R^2}{mf_{\text{PQ}}^2} = 64\pi^2 \frac{f_{\text{PQ}}^2}{M_{\text{Pl}}^2} \tilde{R}^2 \sim 10^{-11}, \quad (51)$$

where we have used $\lambda = m^2/f_{\text{PQ}}^2$ and eqn (31) to estimate R^2 . Hence, the term proportional to λ can be safely neglected and we recover the Poisson equation.

Let us consider the Schwarzschild radius $r_s = 2G_N M$. Using eqs (31) and (32) we obtain

$$\frac{r}{r_s} = \frac{1}{32\pi} \frac{m_{\text{Pl}}^2}{f_{\text{PQ}}^2} \frac{\tilde{r}}{M} \approx 10^{14} \frac{\tilde{r}}{M} \left(\frac{f_{\text{PQ}}}{10^{11} \text{ GeV}} \right)^{-2}. \quad (52)$$

Hence, general relativistic effects are small and the Newtonian treatment of gravity is justified.

References

- [1] For a review, see *e.g.* J. E. Kim, “Light Pseudoscalars, Particle Physics and Cosmology,” *Phys. Rept.* **150** (1987) 1.
- [2] G. G. Raffelt, “Astrophysical methods to constrain axions and other novel particle phenomena,” *Phys. Rept.* **198** (1990) 1.
G. G. Raffelt, “Stars as laboratories for fundamental physics: The astrophysics of neutrinos, axions, and other weakly interacting particles,” Chicago, USA: Univ. Pr. (1996) 664 pp.
- [3] S. Weinberg, “A New Light Boson?,” *Phys. Rev. Lett.* **40** (1978) 223.
F. Wilczek, “Problem of Strong p and t Invariance in the Presence of Instantons,” *Phys. Rev. Lett.* **40** (1978) 279.
- [4] R. D. Peccei and H. R. Quinn, “CP Conservation in the Presence of Instantons,” *Phys. Rev. Lett.* **38** (1977) 1440.
R. D. Peccei and H. R. Quinn, “Constraints Imposed by CP Conservation in the Presence of Instantons,” *Phys. Rev. D* **16** (1977) 1791.
- [5] M. A. Shifman, A. I. Vainshtein and V. I. Zakharov, “Can Confinement Ensure Natural CP Invariance of Strong Interactions?,” *Nucl. Phys. B* **166** (1980) 493.
A. R. Zhitnitsky, “On Possible Suppression of the Axion Hadron Interactions. (In Russian),” *Sov. J. Nucl. Phys.* **31** (1980) 260 [*Yad. Fiz.* **31** (1980) 497].
- [6] M. Dine, W. Fischler and M. Srednicki, “A Simple Solution to the Strong CP Problem with a Harmless Axion,” *Phys. Lett. B* **104** (1981) 199. J. E. Kim, “Weak Interaction Singlet and Strong CP Invariance,” *Phys. Rev. Lett.* **43** (1979) 103.
- [7] M. Dine and W. Fischler, “The Not So Harmless Axion,” *Phys. Lett. B* **120** (1983) 137.
L. F. Abbott and P. Sikivie, “A Cosmological Bound on the Invisible Axion,” *Phys. Lett. B* **120** (1983) 133.
- [8] J. Preskill, M. B. Wise and F. Wilczek, “Cosmology of the Invisible Axion,” *Phys. Lett. B* **120** (1983) 127.
- [9] T. Hiramatsu, M. Kawasaki, K. Saikawa and T. Sekiguchi, “Production of dark matter axions from collapse of string-wall systems,” *Phys. Rev. D* **85** (2012) 105020 [*Phys. Rev. D* **86** (2012) 089902] [arXiv:1202.5851].
- [10] M. Kawasaki, K. Saikawa and T. Sekiguchi, “Axion dark matter from topological defects,” *Phys. Rev. D* **91** (2015) 6, 065014 [arXiv:1412.0789].
- [11] P. Sikivie and Q. Yang, “Bose-Einstein Condensation of Dark Matter Axions,” *Phys. Rev. Lett.* **103** (2009) 111301 [arXiv:0901.1106].
- [12] S. L. Liebling and C. Palenzuela, “Dynamical Boson Stars,” *Living Rev. Rel.* **15** (2012) 6 [arXiv:1202.5809].
- [13] P. Jetzer, “Boson stars,” *Phys. Rept.* **220** (1992) 163.
- [14] T. Rindler-Daller and P. R. Shapiro, “Finding new signature effects on galactic dynamics to constrain Bose-Einstein-condensed cold dark matter,” *Astrophys. Space Sci. Proc.* **38** (2014) 163 [arXiv:1209.1835].
T. Rindler-Daller and P. R. Shapiro, “Angular Momentum and Vortex Formation in Bose-Einstein-Condensed Cold Dark Matter Haloes,” *Mon. Not. Roy. Astron. Soc.* **422** (2012) 135 [arXiv:1106.1256].
T. Rindler-Daller and P. R. Shapiro, “Vortices and Angular Momentum in Bose-Einstein-Condensed Cold Dark Matter Halos,” *ASP Conf. Ser.* **432** (2010) 244 [arXiv:0912.2897].
- [15] P. H. Chavanis, “Mass-radius relation of Newtonian self-gravitating Bose-Einstein condensates with short-range interactions: I. Analytical results,” *Phys. Rev. D* **84** (2011) 043531 [arXiv:1103.2050].
P. H. Chavanis and L. Delfini, “Mass-radius relation of Newtonian self-gravitating Bose-Einstein condensates with short-range interactions: II. Numerical results,” *Phys. Rev. D* **84** (2011) 043532 [arXiv:1103.2054].
- [16] J. Barranco and A. Bernal, “Self-gravitating system made of axions,” *Phys. Rev. D* **83** (2011) 043525 [arXiv:1001.1769].

- [17] C. J. Hogan and M. J. Rees, “Axion Miniclusters,” *Phys. Lett. B* **205** (1988) 228.
- [18] G. Carosi [ADMX Collaboration], “Searching for old (and new) light bosons with the axion dark matter experiment (ADMX),” *AIP Conf. Proc.* **1441** (2012) 494.
- [19] D. M. Jacobs, G. D. Starkman and B. W. Lynn, “Macro Dark Matter,” *Mon. Not. Roy. Astron. Soc.* [arXiv:1410.2236].
- [20] J. Eby, P. Suranyi, C. Vaz and L. C. R. Wijewardhana, “Axion Stars in the Infrared Limit,” *JHEP* **1503** (2015) 080 [arXiv:1412.3430 [hep-th]].
- [21] J. Eby, C. Kouvaris, N. G. Nielsen and L. C. R. Wijewardhana, “Boson Stars from Self-Interacting Dark Matter,” *JHEP* **1602** (2016) 028 [arXiv:1511.04474].
- [22] G. G. di Cortona, E. Hardy, J. P. Vega and G. Villadoro, “The QCD axion, precisely,” arXiv:1511.02867.
- [23] Y. Nambu and M. Sasaki, “Quantum Treatment Of Cosmological Axion Perturbations,” *Phys. Rev. D* **42** (1990) 3918.
- [24] S. Davidson and M. Elmer, “Bose Einstein Condensation of the Classical Axion Field in Cosmology?,” *JCAP* **1312** (2013) 034 [arXiv:1307.8024].
- [25] S. J. Brodsky and P. Hoyer, “The \hbar Expansion in Quantum Field Theory,” *Phys. Rev. D* **83** (2011) 045026 [arXiv:1009.2313].
B. R. Holstein and J. F. Donoghue, “Classical Physics and Quantum Loops,” *Phys. Rev. Lett.* **93** (2004) 201602 [hep-th/0405239].
- [26] F. Dalfovo, S. Giorgini, L. P. Pitaevskii and S. Stringari, “Theory of Bose-Einstein condensation in trapped gases,” *Rev. Mod. Phys.* **71** (1999) 463.
- [27] R. Wald, “General Relativity,” Chicago, USA: Univ. Pr. (1984) 491p, problems of chapter 11.
- [28] I. I. Tkachev, “Coherent scalar field oscillations forming compact astrophysical objects,” *Sov. Astron. Lett.* **12** (1986) 305 [*Pisma Astron. Zh.* **12** (1986) 726].
- [29] J. Binney and S. Tremaine, “Galactic Dynamics”, Princeton University Press, 2008.
- [30] J. Barranco, A. C. Monteverde and D. Delepine, “Can the dark matter halo be a collisionless ensemble of axion stars?,” *Phys. Rev. D* **87** (2013) 103011 [arXiv:1212.2254].
- [31] T. D. Lee and Y. Pang, “Stability of Mini - Boson Stars,” *Nucl. Phys. B* **315** (1989) 477.
- [32] R. L. Davis and E. P. S. Shellard, “Do Axions Need Inflation?,” *Nucl. Phys. B* **324** (1989) 167.
- [33] R. A. Battye and E. P. S. Shellard, “Axion string constraints,” *Phys. Rev. Lett.* **73** (1994) 2954 [*Phys. Rev. Lett.* **76** (1996) 2203] [astro-ph/9403018].
- [34] K. J. Bae, J. H. Huh and J. E. Kim, “Update of axion CDM energy,” *JCAP* **0809** (2008) 005 [arXiv:0806.0497].
- [35] E. W. Kolb and I. I. Tkachev, “Nonlinear axion dynamics and formation of cosmological pseudosolitons,” *Phys. Rev. D* **49** (1994) 5040 [astro-ph/9311037].
E. W. Kolb and I. I. Tkachev, “Axion miniclusters and Bose stars,” *Phys. Rev. Lett.* **71** (1993) 3051 [hep-ph/9303313].
- [36] O. Wantz and E. P. S. Shellard, “Axion Cosmology Revisited,” *Phys. Rev. D* **82** (2010) 123508 [arXiv:0910.1066].
- [37] M. S. Turner, “Cosmic and Local Mass Density of Invisible Axions,” *Phys. Rev. D* **33** (1986) 889.
- [38] R. Kitano and N. Yamada, “Topology in QCD and the axion abundance,” arXiv:1506.00370.

- [39] D. H. Lyth, “Axions and inflation: Sitting in the vacuum,” *Phys. Rev. D* **45** (1992) 3394.
L. Visinelli and P. Gondolo, “Dark Matter Axions Revisited,” *Phys. Rev. D* **80** (2009) 035024 [arXiv:0903.4377].
- [40] G. Aarts and J. Berges, “Classical aspects of quantum fields far from equilibrium,” *Phys. Rev. Lett.* **88** (2002) 041603 [hep-ph/0107129].
- [41] G. Efstathiou, “Cosmological perturbations,” Scottish Universities Summer School in Physics, 24 Jul - 11 Aug 1989. Edinburgh, Scotland
- [42] J. C. Niemeyer and K. Jedamzik, “Dynamics of primordial black hole formation,” *Phys. Rev. D* **59** (1999) 124013 [astro-ph/9901292].
- [43] B. J. Carr, K. Kohri, Y. Sendouda and J. Yokoyama, “New cosmological constraints on primordial black holes,” *Phys. Rev. D* **81** (2010) 104019 [arXiv:0912.5297].
- [44] Kim Griest, Matthew J. Lehner, Agnieszka M. Cieplak, and Bhuvnesh Jain, “Microlensing of Kepler Stars as a Method of Detecting Primordial Black Hole Dark Matter”, *Phys. Rev. Lett.* **107** (2011), 231101
K. Griest, A. M. Cieplak and M. J. Lehner, “New Limits on Primordial Black Hole Dark Matter from an Analysis of Kepler Source Microlensing Data,” *Phys. Rev. Lett.* **111** (2013) 18, 181302.
- [45] E. W. Kolb and I. I. Tkachev, “Femtolensing and picolensing by axion miniclusters,” *Astrophys. J.* **460** (1996) L25 [astro-ph/9510043].
- [46] K. M. Zurek, C. J. Hogan and T. R. Quinn, “Astrophysical Effects of Scalar Dark Matter Miniclusters,” *Phys. Rev. D* **75** (2007) 043511 [astro-ph/0607341].
- [47] Gould, A, “Femtolensing of gamma-ray bursters”, *AP; J* **386** (1992) p. L5-L7.
- [48] G. F. Marani, R. J. Nemiroff, J. P. Norris, K. Hurley and J. T. Bonnell, “Gravitationally lensed gamma-ray bursts as probes of dark compact objects,” *Astrophys. J.* **512** (1999) L13 [astro-ph/9810391].
- [49] A. Barnacka, J. F. Glicenstein and R. Moderski, “New constraints on primordial black holes abundance from femtolensing of gamma-ray bursts,” *Phys. Rev. D* **86** (2012) 043001 [arXiv:1204.2056].
- [50] P. Pani and A. Loeb, “Tidal capture of a primordial black hole by a neutron star: implications for constraints on dark matter,” *JCAP* **1406** (2014) 026 [arXiv:1401.3025].
- [51] A. Barnacka and A. Loeb, “A size-duration trend for gamma-ray burst progenitors,” *Astrophys. J.* **794** (2014) 1, L8 [arXiv:1409.1232 [astro-ph.HE]].
- [52] D. Espriu and A. Renau, “Photons in a cold axion background and strong magnetic fields: polarimetric consequences,” *Int. J. Mod. Phys. A* **30** (2015) 17, 1550099 [arXiv:1401.0663].
D. Espriu and A. Renau, “Photon propagation in a cold axion condensate,” arXiv:1309.6948.
A. A. Andrianov, V. A. Andrianov, D. Espriu and S. S. Kolevator, “Star cooling with pseudoscalar condensates,” arXiv:1507.07087.
- [53] B. J. Carr and M. Sakellariadou, “Dynamical constraints on dark compact objects,” *Astrophys. J.* **516** (1999) 195.
- [54] Hills, J.G., “Limitations on the masses of objects constituting the missing mass in the Galactic disk and the Galactic halo”, *Astronomical Journal*, vol. 92,(1986), p. 595-599.
- [55] R. J. Wilkinson, J. Lesgourgues and C. Boehm, “Using the CMB angular power spectrum to study Dark Matter-photon interactions,” *JCAP* **1404** (2014) 026 [arXiv:1309.7588].
- [56] J. Eby, P. Suranyi and L. C. R. Wijewardhana, “The Lifetime of Axion Stars,” arXiv:1512.01709.
- [57] S. Davidson, “Axions: Bose Einstein Condensate or Classical Field?,” *Astropart. Phys.* **65** (2015) 101 [arXiv:1405.1139].

- [58] A. Iwazaki, “A Possible origin of gamma-ray bursts and axionic boson stars,” Phys. Lett. B **455** (1999) 192 [astro-ph/9903251].
A. Iwazaki, “X-rays from old neutron stars heated by axion stars,” Phys. Lett. B **486** (2000) 147 [hep-ph/9906353].
A. Iwazaki, “Axionic boson stars in magnetized conducting media,” Phys. Rev. D **60** (1999) 025001 [hep-ph/9901396].
- [59] F. Capela, M. Pshirkov and P. Tinyakov, “A comment on ”Exclusion of the remaining mass window for primordial black holes ...”, arXiv:1401.3025,” arXiv:1402.4671.
- [60] F. Capela, M. Pshirkov and P. Tinyakov, “Constraints on primordial black holes as dark matter candidates from capture by neutron stars,” Phys. Rev. D **87** (2013) 12, 123524 [arXiv:1301.4984].
- [61] I. I. Tkachev, “Fast Radio Bursts and Axion Miniclusters,” JETP Lett. **101** (2015) 1, 1 [arXiv:1411.3900 [astro-ph.HE]]. A. Iwazaki, “Fast Radio Bursts from Axion Stars,” arXiv:1412.7825.
- [62] S. Dodelson, “Modern Cosmology,” Academic Press; 1 edition (March 27, 2003).